Thermal Dependence of Thermally Induced Protein Spherulite Formation and Growth: Kinetics of β-lactoglobulin and Insulin

Kristin R. Domike and Athene M. Donald*

Biological and Soft Systems, Cavendish Laboratory, University of Cambridge, United Kingdom

Received August 19, 2007; Revised Manuscript Received October 21, 2007

Amyloid fibril forming proteins have been related to some neurodegenerative diseases and are not fully understood. In some such systems, these amyloid fibrils have been found to form radially oriented spherulite structures. The thermal dependence of formation and growth of these spherulite structures in two model protein systems, β-lactoglobulin and insulin at low pH aqueous and high temperature conditions, have been monitored with time-lapse optical microscopy and quantified. A population-based polymerization reaction model was developed and applied to the experimental data with excellent agreement. While spherulites in the insulin solutions formed and grew at approximately 25× the rate of spherulites in the β-lactoglobulin solutions, the temperature dependence and activation energies of both systems were found to be very similar to one another, suggesting that the underlying rate-limiting mechanisms for both formation and growth are consistent across the two systems. The similarity of both of these amyloid fibril forming protein systems provides confidence in their use as model systems for extrapolating understanding to similar systems involved in neurodegenerative diseases.

Introduction

A number of neurodegenerative diseases have been related to protein aggregation and deposition in the form of amyloid fibrils.[1–10] In some instances, the protein fibrils form more complex agglomerates, such as gels, plaques, or spherulites.[2–4,11–17] Spherulites, the focus of this research, have been found in in vivo tumors and occasionally in diseases such as Alzheimer's and Downs' syndrome.[10,16–21] Analogous to the in vivo aggregates, in vitro fibrillar aggregates also form from proteins and peptides not associated with disease.[22–25] In vitro protein experiments commonly use thermal denaturation to speed aggregation.[22–25] This research study aims to provide insight into the thermal conditions and kinetics of spherulite growth using β-lactoglobulin and insulin as in vitro model systems.

The types of β-lactoglobulin protein aggregates that form in aqueous solutions are dependent upon the conditions. In particular, at pH values near the isoelectric point of ∼5.2, β-lactoglobulin primarily resides in the dimeric form in solution and, over time, forms a network of nearly spherical protein particles referred to as "particulate gels." As the pH moves away from the isoelectric point, long, straight amyloid fibrils form.[26–28] It has been hypothesized that the aggregation of β-lactoglobulin at pH levels far from the isoelectric point initiates from a partially unfolded monomeric form (instead of the dimeric form near the isoelectric pH that results in particulate gels) with an exposed single free cystein Cys-121, which can bind in intermolecular disulfide bonds and create ordered linear fibrils.[29,30] Atomic force microscopy has been used to visualize β-lactoglobulin fibrils formed at low pH, and unbranched fibrils have been found with dimensions of ∼0.1–2.0 μm in length and 8.5 ± 1.4 nm in width.[31] The fibrils aggregate into "fine strand gels" that have the same type of intramolecular hydrogen bonds on both sides of the isoelectric range as measured by FTIR.[30] It is in these solution conditions that spherulites composed of radially oriented, amyloid fibrils have been found with the highest concentrations of spherulites around pH levels of 1.5 and 7.5.[26] The spherulites that form are reported as not being reversibly destroyed by dilution, alteration of solution conditions, or modest shear forces during pipetting.[26]

Aggregation of β-lactoglobulin can be induced and accelerated by heating. Upon heating of β-lactoglobulin in solution at low pH, there is an onset of denaturation and shift toward monomeric form beginning at 60 °C as measured by FTIR. After this denaturation, fibril formation begins.[30] The total heating time required for fibril formation in a β-lactoglobulin solution has been reported to be not affected by heat interruption.[26]

Similarly, aqueous solutions of insulin protein have been found to form spherulites at low pH conditions. Fully formed insulin spherulites are notably different from β-lactoglobulin spherulites in that they have a significantly sized central core of irregularly oriented, nonamyloid protein. Radially oriented amyloid fibrils exist outside the amorphous core.[32–34] As the onset of growth of fibrils in the solution and that of spherulites occurred at similar times, it was suggested that the spherulites grow from small precursors and are not assembled from pre-existing fibrils in solution.[32] Both the initial appearance time and the growth of the radius of the full spherulite (core and fibrils) have been monitored as a function of temperature for insulin spherulites for 65, 70, and 75 °C and found to occur faster with increasing temperature. In these experiments, the spherulites were described as growing linearly or slightly faster than linearly and then suddenly ending their growth at the same time, suggested to be caused by the sudden depletion of precursors.[34] Furthermore, sedimentation velocity experiments of insulin spherulites of various sizes were also carried out, with the results of these experiments indicating that the insulin spherulites are of constant density independent of size. This constant density was suggested as being caused by branching of the fibrils that radiate from the insulin amorphous core.[34]

Other studies monitoring the kinetics of amyloid fibril growth of both β-lactoglobulin and insulin have qualitatively found that the kinetics follow a "lag time, growth, plateau" pattern.[26,28,32,35] The growth has been described quantitatively using a nucleated polymerization reaction mechanism.[36,37] Growth of spherulite

* Corresponding author. E-mail: amd3@cam.ac.uk.

10.1021/bm7009224 CCC: $37.00 © 2007 American Chemical Society
Published on Web 11/27/2007

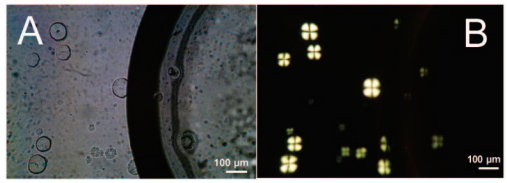

Figure 1. Optical microscopy images at 50× of fully grown spherulites of β-lactoglobulin: (A) without cross-polarizers; (B) with cross-polarizers. It is possible to differentiate spherulites and bubbles and show that the thick black line visible in (A) is a bubble.

structures has qualitatively been found to follow similar type of kinetics.[29] It is the objective of this research to monitor and quantify the growth of β-lactoglobulin and insulin spherulites over a range of incubation temperatures.

Experimental Method

The two proteins used in this research were obtained from Sigma-Aldrich (Gillingham, UK) and are of analytical grade: β-lactoglobulin (product number L0130; mixture of types A and B) and bovine insulin (product number I5500). Protein solutions were made by dissolving the protein in distilled and deionized water. The desired pH was achieved by adding 1 M HCl (Sigma-Aldrich) in 5–50 μL increments. Glass slides with wells were filled with 100 μL of protein solution, covered with a glass coverslip, and heated to the required temperature on a heating stage placed within the Zeiss Axioplan optical microscope (Carl Zeiss Ltd., Welwyn Garden City, UK). Total magnification of either 50× or 100× was used. A polarizer and analyzer were put in fixed positions, orthogonal to one another for the cross-polarizer imaging. Time-lapse and still images were taken using a Kodak digital camera mounted on the top of the microscope. The size of spherulites seen in the images was determined by calibrating with a scale bar of known dimension and thereby quantifying the spatial resolution per pixel image. Images of β-lactoglobulin solutions were taken at 50× magnification for which the resolution was 1.56 μm/pixel; spherulites could not be distinguished with radii less than 10 μm. Insulin spherulites were significantly smaller than those of β-lactoglobulin, and therefore, images of the insulin solutions were taken with a higher magnification of 100× for which the resolution was 0.78 μm/pixel and 5 μm was the minimum spherulite radius that could be resolved with confidence.

The crossed-polarizer optical microscopy allows for the monitoring of spherulites. Example images of fully grown β-lactoglobulin spherulites without and with cross-polarizers are shown in Figure 1. Use of the cross-polarizers serves three purposes: (1) allows for the differentiation of spherulites and bubbles; (2) enables identification of overlapping spherulites; (3) the cross-pattern found in all spherulites viewed with cross-polarizers suggests that the internal structure of each spherulite is radially oriented.[32]

In an attempt to provide an estimate of the time required to bring all of the protein solution to the temperature of the heating stage, a two-dimensional transient heat transfer by conduction finite element simulation was run in COMSOL Multiphysics (COMSOL Ltd., Hertfordshire, UK). The experimental setup of the slide and slide cover on the heating stage are shown in Figure 2. Relevant physical properties (heat capacity, heat transfer coefficient, and density) of each material (glass, air, solution simulated as water) were imported from the standard COMSOL material library. A boundary condition was used for each of the four external boundaries: the bottom was simulated as the hot plate increasing from 293 to 353 K in the first minute (based on empirical measurement) and then staying at 353 K; left, top, and right were simulated as having very slow convection heat loss to the surrounding. The simulation calculated that the entire system was at steady state temperature of 353 K within three minutes. This time to thermal equilibrium is short compared to the earliest appearance of spherulites in the protein solutions except in the fastest forming conditions (insulin at 80 °C), and so this time offset is ignored from here on.

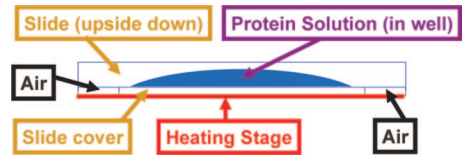

Figure 2. Experimental setup for heating of protein solutions during time-lapse optical imaging with materials shown. This same setup was used for the finite element modeling that simulates the entire system comes to steady-state temperature within 3 min of the heat stage being switched on.

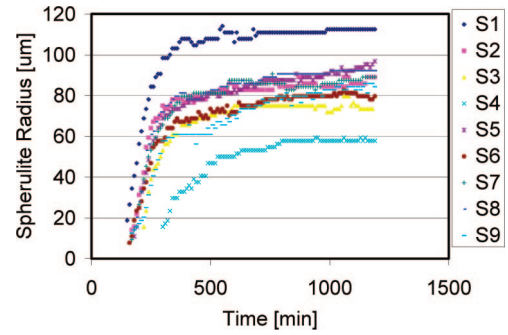

Figure 3. Radii measurements over the first 1190 min of growth for nine spherulites incubated at 85 °C of a 4 wt % β-lactoglobulin solution in the field of view.

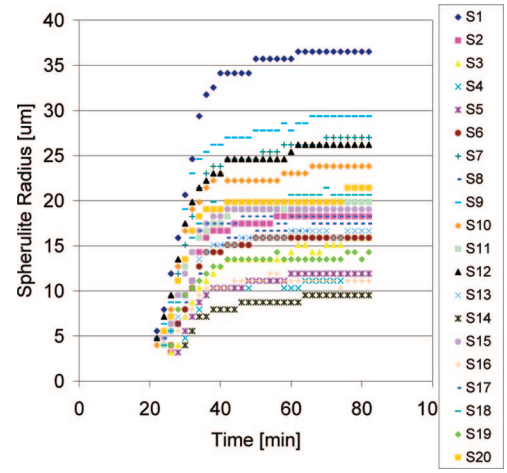

Figure 4. Radii measurements over the first 82 min of growth for 20 spherulites incubated at 75 °C of a 1 wt % insulin solution in the field of view.

Results and Discussion

Pattern of Spherulite Growth. By capturing crossed-polarizer optical microscopy images and measuring the radius of each spherulite in the field of view at regular time intervals, the growth of spherulites was monitored. Resulting growth curves from one experiment for nine separate β-lactoglobulin spherulites in the field of view during incubation at 85 °C of a 4 wt % β-lactoglobulin solution are presented in Figure 3. Similarly, growth curves for 20 insulin spherulites during incubation at 75 °C of a 1 wt % insulin solution are presented in Figure 4. The spherulite growth patterns in the two figures are similar to one another and are representative of all the experiments of both types of proteins performed in this research. They all share the following four characteristics: (1) a time lag before spherulite

CDV

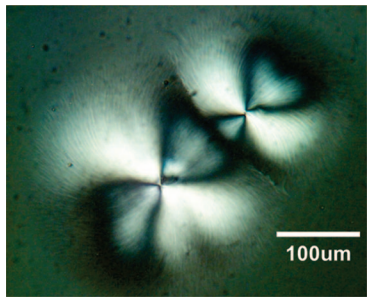

Figure 5. Optical microscopy image of two fully grown spherulites of β-lactoglobulin.

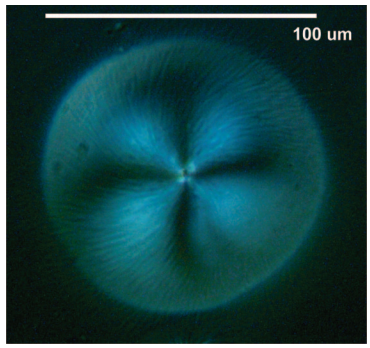

Figure 6. Optical microscopy image of a fully grown spherulite of β-lactoglobulin.

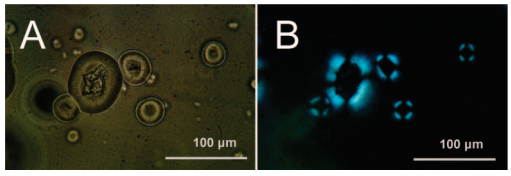

Figure 7. Optical microscopy images at 100× magnification of fully grown spherulites of insulin: (A) without cross-polarizers; (B) with cross-polarizers.

are seen; (2) an initial rapid growth of the spherulite, followed by a gradual decrease in the growth rate of the spherulites; (3) the growth rate at any given time is similar for different spherulites in the same experiment; (4) there is significant variability in the duration of the time lag for different spherulites. These characteristics are consistent with the "lag time, growth, plateau" growth pattern seen in other amyloid fibril systems.[26,28,32,35]

A high resolution optical microscopy image of two grown spherulites of β-lactoglobulin is presented in Figure 5. In this image, the radially oriented internal structure appears to be strands of fibril bundles (because individual fibrils are too narrow to be seen optically) with slight curvature to their orientation and without obvious branching. This is particularly viewable at the outer edges of the spherulites, where the fibril bundles are slightly separated from one another. Another image of a fully grown spherulite of β-lactoglobulin is presented in Figure 6, and the internal structure appears similar to the structure of the spherulites presented in Figure 5.

Sample images of fully grown insulin spherulites are presented in Figure 7. Unlike the β-lactoglobulin spherulites, the insulin spherulites have relatively large cores that demonstrate no radial structure when viewed with cross-polarizers, as demonstrated in Figure 8B.

Some previous discussions and models of insulin spherulite growth have assumed or suggested that the nonradially oriented core is a nucleus that forms first followed by a radially ordered outer ring.[32,34] However, monitoring both the core size and total

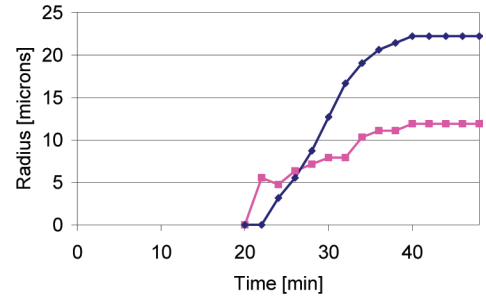

Figure 8. Growth of the radius of the radially oriented fibrils and of the radius of the core for a insulin spherulite incubated at 75 °C, where -■- is the radial fibril length and -●- is the core radius.

Table 1. Final Average Full Spherulite, Spherulite Core, and Radial Fibril Sizes of 20 Insulin Spherulites

	final spherulite radius		final core radius		final radial fibril length	
temperature	average [μm]	RSD [%]	average [μm]	RSD [%]	average [μm]	RSD [%]
65 °C	14.8	33	5.99	56	8.77	24
70 °C	17.3	35	8.33	48	8.93	31
75 °C	19.2	35	11.19	42	8.06	29
80 °C	12.6	25	6.19	36	6.43	15

spherulite size using time-lapse optical microscopy with cross-polarisers shows that the radially oriented fibrils appear before the core appears in view and that both grow simultaneously throughout the full duration of insulin spherulite growth. A sample plot of growth of both core radius and radius length of the radially oriented section of the insulin spherulite is presented in Figure 8. The radially oriented fibrils appear before the core and grow to be approximately 11 μm in length, while the core radius increases to 22 μm in length. The radially oriented fibrils and the core both come to a steady-state, final length at the same time. That the core continues to grow throughout this time period was not detected in the earlier work,[34] which only used differential interference contrast, with which the size of the core could not be determined. However, its growth is clearly of significance. Although a definitive explanation as to why the core grows cannot be proposed, one possible hypothesis is that the fibrils are not sufficiently stiff to remain correctly oriented as they grow in length. In this scenario, the individual fibrils would therefore collapse under compression as the whole spherulite increases in size, losing orientation and therefore birefringence. In this case, the core would contain misaligned fibrils. Collapsing fibrils into a core also could explain the approximately constant density previously found among insulin spherulites by rheological experiments.[34] Further work is necessary to confirm or repudiate the hypothesis.

The average final sizes and intraexperimental variability (quantified by the associated relative standard deviation, RSD) of all of the insulin spherulites, their cores, and outer ring of radial fibrils are presented in Table 1 for all temperatures investigated. For all temperatures, there is significant intraexperimental variability in the core size, while, as stated above, the final outer ring length remains relatively constant in length. Across temperatures, as the final spherulite radius increases or decreases, the outer ring length remains relatively consistent in length. These observations suggest that the radially oriented fibrils approach some threshold length (which is dependent on the spherulite size but has an average maximum length of approximately 9 μm) and the sections of the fibrils in the center of the insulin spherulite lose their radial orientation and form

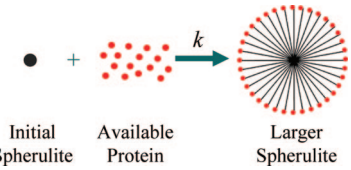

Figure 9. Schematic model of spherulite growth by addition of available protein.

the core at each temperature. Variability of these sizes between spherulites within an experiment are quantified and presented as relative standard deviation (RSD).

Theoretical Model and Data Fit Methodology. On the basis of the growth pattern observed and analysis of previous research in modeling fibril growth, a growth model of linear polymerization for a population of spherulites was applied. This model is similar to the polymerization model for the growth of insulin spherulites recently presented by Rogers et al.[34] with the following two observational amendments:

1. The spherulite growth curves in this research are observed to approach steady state gradually as opposed to the sudden stop hypothesis presented by Rogers et al.[34]

a. Review of the growth curves presented by Rogers et al.[34] suggests the approach dynamics to steady state are either unclear due to very rapid (at high temperatures) with low resolution data (optical images taken every few minutes) or clearly gradual for all lower temperature growth curves and growth of seeded solutions.

b. Gradual approach to steady state is consistent with previous observations of amyloid fibril growth.[26,28,32,35]

2. The amorphous insulin core within the spherulite grows as the radially oriented fibrils grow, and not simply prior to the radially oriented fibrils growth as proposed by Rogers et al.[34]

a. This new observation eliminates the requirement proposed by Rogers et al.[34] that the outer insulin fibrils branch as they grow in order to have spherulites of nearly constant density.

In this polymerization model, each spherulite, i, is modeled as appearing in the optical field of view at an appearance time, $t_{A,i}$, and then the radius of the spherulite grows with the addition of available protein attaching to the exposed fibril ends. This polymerization reaction at the exposed fibril ends proceeds at an overall rate proportional to a temperature-dependent rate constant, k, and proportional to the concentration of protein available in the surrounding solution, $[P]_i$. The resulting equation for growth of a single spherulite radius, $R_{S,i}$, is presented in eq 1. In allowing the concentration of available protein around each spherulite to decrease at its own rate but holding the growth rate constant of fibril growth, k, constant for all spherulites in the experiment, an implicit assumption is made that the underlying mechanism of fibril growth is consistent for the different spherulites in any given experiment and that the temperature throughout the solution is relatively uniform. The appearance time and local available protein concentration depletion rate, $d_{P,i}$, were allowed to vary for each spherulite. The local concentration for each spherulite was modeled as single-source first-order depletion as presented in eq 2. Possible sources of variability in this depletion rate between different spherulites in solution include local consumption of available protein for the growth of other nearby spherulites and initial spatial inconsistencies in concentration. The details of nucleation prior to appearance in the optical view field are not explicitly modeled in this work as the details were not visible with the optical techniques employed. A pictorial representation of this first-order polymerization reaction is presented in Figure 9.

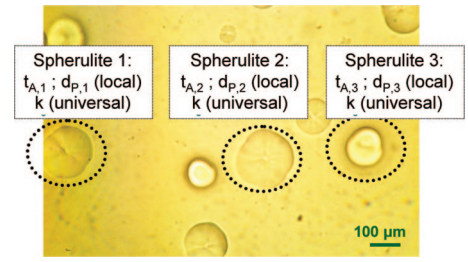

Figure 10. Parameters to fit growth of population of spherulites.

Although the fibrils in the resulting spherulite are depicted as perfectly radial, the internal ordering of the fibrils is dependent upon the protein and the spherulite size. Specifically, in the case of β-lactoglobulin, the internal ordering remains radial with some possible tendency toward slight curvature of the fibril strands. Specifically, in the case of insulin, an amorphous (no systematic orientation) core grows inside of the spherulite while the outer section remains radially oriented. The transformation of radially oriented fibrils into the amorphous core is not explicitly modeled as significantly altering the overall spherulite radius.

$$\frac{dR_{S,i}}{dt} = \begin{cases} 0 & \text{for } t \le t_{A,i} \\ k[P_i(t)] & \text{for } t > t_{A,i}. \end{cases} \quad (1)$$

$$P_i(t) = P_i(t_{A,i}) \exp(-d_{p,i}(t - t_{A,i})) \quad (2)$$

Explicitly, the parameters used to fit the growth of a population of three spherulites are shown in .Figure 10. For an experiment that has n spherulites in the field of view, $2n + 1$ parameters (n appearance times, n available protein depletion rates, and a single fibril growth rate) are selected to provide the best fit of the model to the data of the growth of all of the spherulites.

The experimental extent of variability in available local protein concentration can be visualized by plotting the change in spherulite radii over time for spherulites within a population. An example of this variability can be seen in the 100 min moving average solid lines of Figure 11B. While all rates of change in the spherulite radius are following an exponential decay as expected in a first-order reaction, at least two of the spherulites (S1 and S4) have growth rates significantly faster than the other spherulites at the time that those two spherulites first appear. In contrast, two other late forming spherulites (S2 and S3) have growth rates nearly identical to the others at the time of their first appearance.

An example of the model fit to the data is presented in Figure 12A for the same experimental data as that displayed in Figure 3. The model is depicted as a solid line, and the raw data as points at 10 min intervals. The calculated local available protein concentrations for all nine spherulites, which are modeled as depleting at independent logarithmic rates, are presented in Figure 12B. The calculated local available protein concentrations for the different spherulites are very similar to one another, with the exception of the single late-appearing spherulite (S6) depleting at a similar rate but later than the other spherulites. This difference in local calculated concentration of available protein for S6 compared to the other spherulites suggests that the concentration of BLG protein can vary throughout the solution and that diffusion across length scales of spherulite separation in these experimental conditions is slow relative to the polymerization reaction. This indicates that diffusion is likely controlling the rate of aggregation under these conditions more than the polymerization reaction, i.e., it is not in general CDV

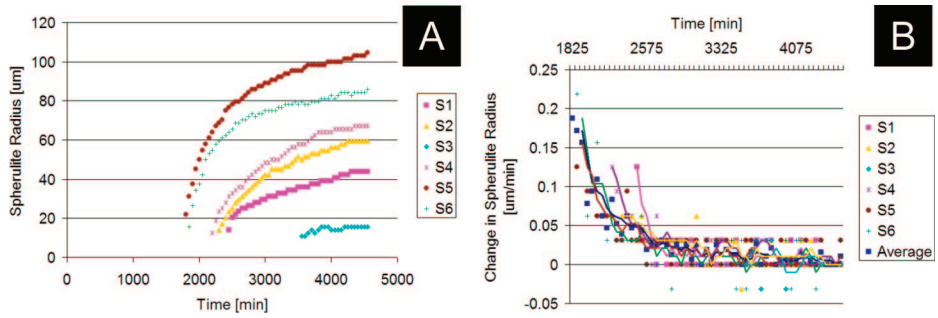

Figure 11. (A) Spherulite radii and (B) change in spherulite radii for six spherulites of β-lactoglobulin incubated at 60 °C for 4550 min with solid lines indicating 100 min moving averages.

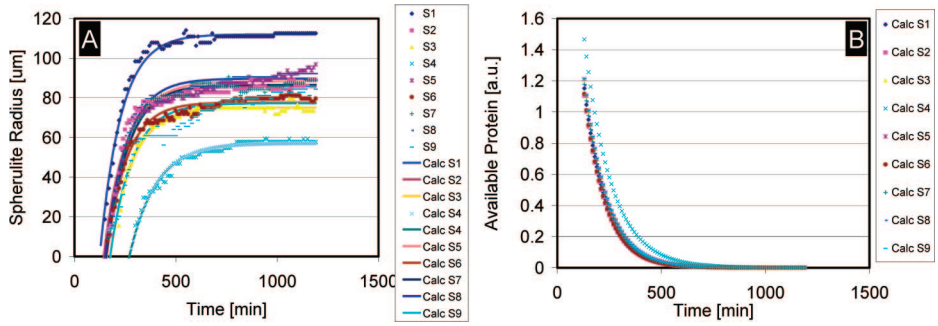

Figure 12. (A) Linear polymerization model for radii measurements over the first 1190 min of growth for nine β-lactoglobulin spherulites at 85 °C and 4 wt % in the field of view. (B) Calculated available protein available for spherulite growth in the polymerization model for the same nine β-lactoglobulin spherulites at 85 °C and 4 wt %.

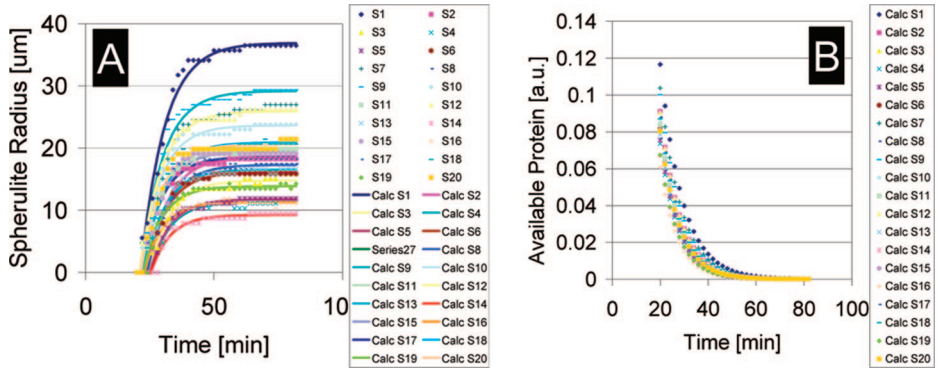

Figure 13. (A) Linear polymerization model for radii measurements over the first 82 min of growth for 20 spherulites at 75 °C and 1 wt % in the field of view. (B) Available protein available for spherulite growth in the polymerization model for 20 insulin spherulites at 75 °C and 1 wt %.

reaction-limited aggregation.. Further experiments over a range of different initial protein concentrations could be conducted to empirically determine the relative rates of local diffusion and the polymerization reaction. An analogous data set for a 1 wt % insulin solution incubated at 75 °C is displayed in Figure 13 with similar uniformity of calculated available protein depletion. The spherulite appearance times in this insulin experiment are all very similar (within 5 min of one another) and therefore do not provide insight into the relative rate of movement of available protein between spherulite locations. We note that insulin is a much smaller molecule than BLG and is therefore less likely to be diffusion limited. This may (at least in part) explain why the range of conditions for insulin that were explored in ref 34 show an apparent switch between the two mechanisms that is not being picked up in the current study and why, for BLG, the dominant effect appears to be diffusion-limited aggregation.

Across the many experiments and multiple protein systems, the model residuals (the difference between the model and the data) did not demonstrate systematic patterns. This lack of systematic patterns provides confidence in the models ability to accurately describe the data. The details of this analysis are not shown.

Effect of Temperature on Spherulite Growth of β-Lactoglobulin. Solutions of β-lactoglobulin at pH 1.57−1.59 and 4 wt % concentration were incubated at temperatures of 60, 70, 80, 85, and 90 °C. Three experiments at each temperature were completed to provide an estimate of reproducibility of the resulting data. The linear polymerization model was independently applied to each experiment. The resulting model parameters of minimum appearance time, mean appearance time, relative standard deviation of appearance time, and spherulite growth rate, k, for all of the β-lactoglobulin experiments are presented in Table 2. Despite the small number of spherulites in the field of view of each experiment at the lower temperatures, the reproducibility of the mean value of the parameters between experiments at a given temperature was sufficiently high to discern differences between experiments at the different temperatures. Appearance times (minimum and mean) decrease with increasing temperature, while the spherulite growth rate i

GDV

Table 2. Parameters from Linear Polymerization Model for All β-Lactoglobulin Experiments

solution temperature	number of spherulites	appearance time [min] minimum	appearance time [min] mean	appearance time [min] RSD [%]	spherulite growth rate [μm/(wt %* min)]
60 °C	6	1651	2051	16	5.29×10^{-2}
60 °C	4	947	1698	30	4.09×10^{-2}
60 °C	3	2336	3287	29	7.60×10^{-3}
70 °C	6	653	835	16	8.93×10^{-2}
70 °C	4	1030	1075	5	5.13×10^{-2}
70 °C	5	754	1080	29	6.27×10^{-2}
80 °C	9	240	431	35	3.40×10^{-1}
80 °C	7	241	374	28	1.82×10^{-1}
80 °C	6	207	300	31	2.16×10^{-1}
85 °C	9	132	169	22	3.18×10^{-1}
85 °C	9	147	205	27	4.71×10^{-1}
85 °C	11	130	161	16	3.51×10^{-1}
90 °C	14	72	108	26	3.96×10^{-1}
90 °C	4	65	106	38	6.94×10^{-1}
90 °C	3	84	97	12	5.90×10^{-1}

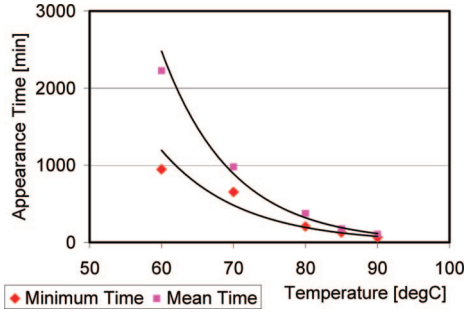

Figure 14. Temperature dependence of minimum and mean appearance times for all β-lactoglobulin experiments with exponential curve fits shown as solid curves. The R^2 value (a metric of quality of fit) for the minimum appearance time exponential curve is 0.96 and for the mean appearance time is 0.99.

creases with temperature. The relative standard deviation of the appearance time between spherulites within a given experiment has no dependence on solution temperature.

There are distinct differences in both the mean and minimum appearance times of the β-lactoglobulin experiments at different temperatures, as displayed in Figure 14, with the data displayed with fitted exponential curves.

Effect of Temperature on Spherulite Growth of Insulin. Solutions of 1 wt % concentration insulin at pH 1.57–1.59 and 1 wt % were incubated at temperatures of 65, 70, 75, and 80 °C. A single experiment was performed at each temperature as there were in excess of 20 spherulites in the field of view in all experiments. The resulting growth curves of the outer radii of the spherulites and model fits are presented for all experiments in Figure 15. As with β-lactoglobulin, the insulin spherulites appear significantly earlier and grow faster at higher temperatures. The model provides excellent fit to the vast majority of insulin spherulites. The exceptions to the excellent agreement between data and model are the first spherulites to form at the two lower temperatures. These spherulites appear to follow a growth curve of different shape than the growth predicted by the linear polymerization model. However, analysis of the model residuals (not shown) demonstrates that no systematic error between model and data exists.

The resulting parameters for the model fit for all of the insulin experiments are presented in Table 3. Compared to the β-lactoglobulin experiments, insulin forms spherulites much faster, with a greater population density in the solution, and have significantly smaller variability between appearance times within an experiment (demonstrated by the RSD). The spherulite growth occurs about 25 times faster in insulin than β-lactoglobulin; at 70 °C, an insulin spherulite takes about one hour to fully form, compared to one day for β-lactoglobulin. Consistent with β-lactoglobulin, the temperature dependence of both the minimum and mean appearance times follow an exponential curve, as shown in Figure 16.

Comparison of Temperature Dependence on Rates between the Two Protein Systems. The smaller insulin protein molecules form spherulites and grow at rates significantly faster than the larger β-lactoglobulin. However, the spherulite formation and growth rates of the two protein systems have similar relative responses to temperature. For example, when the temperature increases from 70 to 80 °C, the mean appearance time decreases by approximately 65% in both systems and the growth rate increases by a factor of approximately 3. This similar relative response to temperature is demonstrated in an Arrhenius plot of the inverse of mean appearance time (which is proportional to creation rate) displayed in Figure 17. The similarity of the associated slopes of the linear fits demonstrate that the polymerization reactions of the two protein systems have very similar temperature dependence profiles. The similar responses to temperature of the two reacting systems suggest that the underlying mechanism in the spherulite creation is similar in the two systems and that the difference in magnitude of the overall reaction rates between the two systems is due to differences in the pre-exponential factor in the Arrhenius equation. This is likely, as indicated above, to be due to the very different sizes of the two molecules. Additionally, the Arrhenius plot of the spherulite growth rate constant displayed in Figure 18 and the associated slopes of the linear fits demonstrate similarity between the mechanism of spherulite growth in both reactions, suggesting that the underlying mechanism is similar in both systems. Activation energies were calculated directly from the slopes of the Arrhenius plot and were found to be 17 kcal/mol for the insulin spherulite growth and 24 kcal/mol for the BLG spherulite growth. These values are similar to recently reported activation energy values for insulin fibril growth of 24 kcal/mol[38] and 25 kcal/mol.[39]

Conclusions

Time-lapse optical microscopy under polarized light was used to monitor and quantify growth of spherulite structures in thermally induced aggregating protein solutions for both β-lactoglobulin and insulin at low pH aqueous conditions. The β-lactoglobulin spherulites that formed were composed entirely of radially oriented fibrils. The insulin spherulites also expanded with radial growth but were found to have a nonbirefringent core in the center of the spherulite, which itself grew as the spherulites grew. The insulin amorphous core had previously been incorrectly identified as a precursor nucleus that fully formed in advance of the radially oriented outer shell of the spherulite.

A population-based polymerization model was fit to the spherulite growth data and found to have excellent agreement with data from both protein solutions. The model allowed for the quantification of the population spherulite growth rate and the appearance time for each spherulite in the population. This type of model is consistent with models used to describe other aggregating fibril systems. Confidence in the model was demonstrated determining that no systematic patterns in the model residuals existed.

Use of the quantitative population growth and appearance times to compare the temperature dependence of β-lactoglobulin

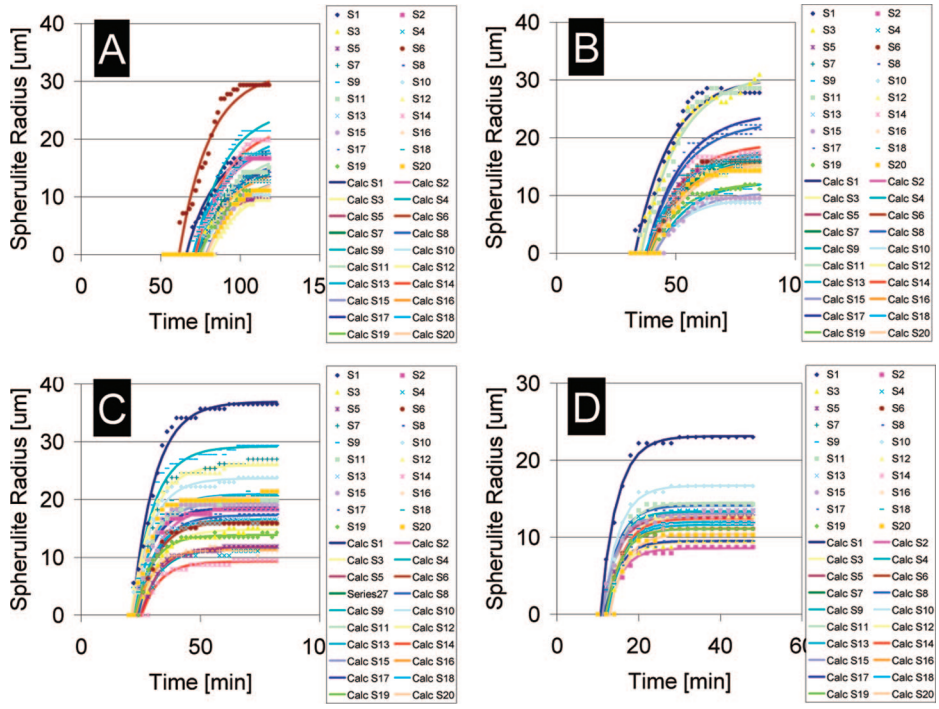

Figure 15. Growth curves of insulin spherulites with data shown as points and linear polymerization model shown as solid lines: (A) 65 °C; (B) 70 °C; (C) 75 °C; (D) 80 °C.

Table 3. Parameters from Linear Polymerization Model for All Insulin Experiments

solution temperature	number of spherulites	appearance time [min]			spherulite growth rate [μm/(wt % min)]
		minimum	mean	RSD [%]	
65 °C	20	58	72	7	1.99
70 °C	20	31	38	8	2.31
75 °C	20	20	23	7	3.47
80 °C	20	11	12	6	5.85

spherulite formation and growth to that of insulin provided insight that rates in both solutions have exponential temperature dependence and have similar activation energies to each other and to the previously reported activation energy for insulin fibril formation (not within spherulites). This result suggests that the underlying rate-limiting mechanisms for both formation and growth are similar in both systems and similar to nonspherulite fibril formation. The similarity of both of these amyloid fibril forming protein systems provides confidence in their use as model systems for extrapolating understanding to similar systems, such as those involved in neurodegenerative diseases.

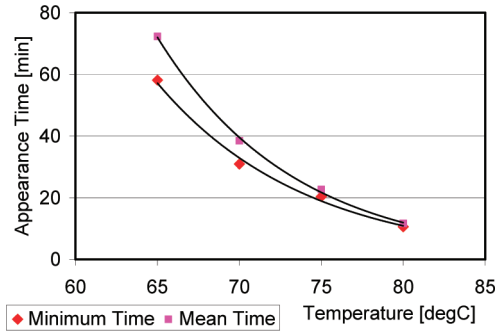

Figure 16. Temperature dependence of minimum and mean appearance times for all insulin experiments with exponential curve fits shown as solid curves. The R^2 value (a metric of quality of fit) for the minimum appearance time curve is 0.99 and for the mean appearance time is 1.00.

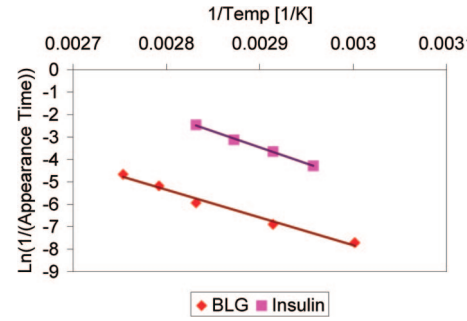

Figure 17. Arrhenius plot of spherulite creation rate for β-lactoglobulin (BLG) and insulin systems with linear trendlines. The slope of the linear trendline for the BLG data is −12 300 with a R^2 value of 0.99. The slope of the linear trendline for the insulin data is −14 300 with a R^2 value of 1.00.

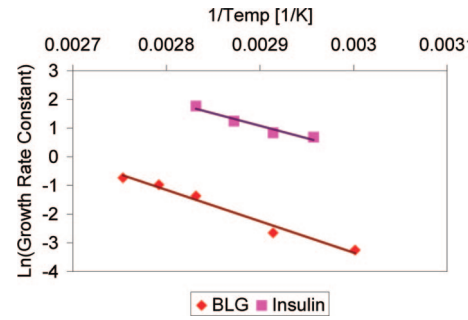

Figure 18. Arrhenius plot of spherulite growth rate constant for β-lactoglobulin and insulin systems with linear trendlines. The slope of the linear trendline for the BLG data is −10 900 with a R^2 value of 0.98. The slope of the linear trendline for the insulin data is −8670 with a R^2 value of 0.94.

Acknowledgements. We thank the EPSRC for funding and the collegial contributions in training and insight of past and present Cavendish Laboratory members, particularly Mark Krebs, Salman Rogers, Beth Bromley, and Debra Lin. CDV

References and Notes

(1) Sunde, M.; Blake, C. *Adv. Protein Chem.* **1997**, *50*, 123–159.
(2) Uversky, V. N.; Segel, D. J.; Doniach, S.; Fink, A. L. *Proc. Natl. Acad. Sci. U.S.A.* **1998**, *95*, 5480–5483.
(3) Fink, A. L. *Fold. Des.* **1998**, *3*, 9–23.
(4) Bauer, R.; Carrotta, R.; Rischel, C.; Ogendal, L. *Biophys. J.* **2000**, *79*, 1030–1038.
(5) Kelly, J. W. *Curr. Opin. Struct. Biol.* **1998**, *8*, 101–106.
(6) Sigurdsson, E. M.; Wisniewski, T.; Frangione, B. *Trends Mol. Med.* **2002**, *8*, 411–413.
(7) Dobson, C. M. *Nature* **2003**, *426*, 884–890.
(8) Westermark, P.; Benson, M. D.; Buxbaum, J. N.; Cohen, A. S.; Frangione, B.; Ikeda, S.; Masters, C. L.; Merlini, G.; Saraiva, M. J.; Sipe, J. D. *Amyloid* **2002**, *9*, 197–200.
(9) Uversky, V. N.; Fink, A. L. *Biochim. Biophys. Acta* **2004**, *1698*, 131–153.
(10) Sipe, J. D. *Annu. Rev. Biochem.* **1992**, *61*, 947–975.
(11) Goldstein, R. F.; Stryer, L. *Biophys. J.* **1986**, *50*, 583–599.
(12) Oosawa, F.; Kasai, M. *J. Mol. Biol.* **1962**, *4*, 10–21.
(13) Flyvbjerg, H.; Jobs, E.; Leibler, S. *Proc. Natl. Acad. Sci. U.S.A.* **1996**, *93*, 5975–5979.
(14) Saville, B. *J. Phys. Chem.* **1971**, *75*, 2215–2217.
(15) Sipe, J. D.; Cohen, A. S. *J. Struct. Biol.* **2000**, *130*, 88.
(16) Jin, L. W.; Claborn, K. A.; Kurimoto, M.; Geday, M. A.; Maezawa, I.; Sohraby, F.; Estrada, M.; Kaminksy, W.; Kahr, B. *Proc. Natl. Acad. Sci. U.S.A.* **2003**, *100*, 15294.
(17) Acebo, E.; Mayorga, M.; Val-Bernal, J. F. *Pathology* **1999**, *31*, 8–11.
(18) Taniyama, H.; Kitamura, A.; Kagawa, Y.; Hirayama, K.; Yoshino, T.; Kamiya, S. *Vet. Pathol.* **2000**, *37*, 104–107.
(19) Vos, J. H.; Gruys, E. *Vet. Pathol.* **1985**, *22*, 347–354.
(20) Manuelidis, L.; Fritch, W.; Xi, Y. G. *Science* **1997**, *277*, 94–98.
(21) Snow, A. D.; Sekiguchi, R.; Nochlin, D.; Fraser, P.; Kimata, K.; Mizutani, A.; Arai, M.; Schreier, W. A.; Morgan, D. G. *Neuron* **1994**, *12*, 219–234.
(22) Burke, M. J.; Rougvie, M. A. *Biochemistry* **1972**, *11*, 2435–2439.
(23) Beaven, G. H. *Eur. J. Biochem.* **1969**, *11*, 37–42.
(24) Davidson, B.; Fasman, G. D. *Biochemistry* **1967**, *6*, 1616–1629.
(25) Clark, A. H.; Judge, F. J.; Richards, J. B.; Stubbs, J. M.; Suggett, A. *Int. J. Pept. Protein Res.* **1981**, *17*, 380–392.
(26) Bromley, E. H. C.; Krebs, M. R. H.; Donald, A. M. *Faraday Discuss.* **2005**, *128*, 13–27.
(27) Kavanagh, G. M.; Clark, A. H.; Ross-Murphy, S. B. *Int. J. Biol. Macromol.* **2000**, *28* (1), 41–50.
(28) Arnaudov, L. N.; de Vries, R. *Biomacromolecules* **2003**, *4*, 1614–1622.
(29) Vetri, V.; Militello, V. *Biophys. Chem.* **2005**, *113*, 83–91.
(30) Lefevre, T.; Subirade, M. *Biopolymers* **2000**, *54*, 578–586.
(31) Gosal, W. S.; Clark, A. H.; Ross-Murphy, S. B. *Biomacromolecules* **2004**, *5*, 2408–2419.
(32) Krebs, M. R. H.; Bromley, E. H. C.; Rogers, S. S.; Donald, A. M. *Biophys. J.* **2005**, *88*, 2013–2021.
(33) Krebs, M. R. H.; MacPhee, C. E.; Miller, A. F.; Dunlop, I. E.; Dobson, C. M. *Proc. Natl. Acad. Sci. U.S.A.* **2004**, *101*, 14420–14424.
(34) Rogers, S. S.; Krebs, M. R. H.; Bromley, E. H. C.; Linden, E.; Donald, A. M. *Biophys. J.* **2006**, *90*, 1043–1054.
(35) Majhi, P. R.; Ganta, R. R.; Vanam, R. P.; Seyrek, E.; Giger, K.; Dubin, P. *Langmuir* **2006**, *22*, 9150–9159.
(36) Kodaka, M. *Biophys. Chem.* **2004**, *109*, 325–332.
(37) Powers, E. T.; Powers, D. L. *Biophys. J.* **2006**, *91*, 122–132.
(38) Knowles, T. P. J.; Shu, W.; Devlin, G. L.; Meehan, S.; Auer, S.; Dobson, C. M.; Welland, M. E. *Proc. Natl. Acad. Sci. U.S.A.* **2007**, *104* (24), 10016–10021.
(39) Mauro, M.; Craparo, E. F.; Podesta, A.; Bulone, D.; Carrotta, R.; Martorana, V.; Tiana, G.; San Biagio, P. L. *J. Mol. Biol.* **2007**, *366*, 258–274.

BM7009224